



# Glacial freshwater discharge events recorded by authigenic neodymium isotopes in sediments from the Mendeleev Ridge, western Arctic Ocean



Kwangchul Jang<sup>a</sup>, Yeongcheol Han<sup>a</sup>, Youngsook Huh<sup>a,\*</sup>, Seung-Il Nam<sup>b</sup>, Ruediger Stein<sup>c</sup>, Andreas Mackensen<sup>c</sup>, Jens Matthiessen<sup>c</sup>

<sup>a</sup> School of Earth and Environmental Sciences, Seoul National University, Seoul 151-747, South Korea

<sup>b</sup> Division of Polar Climate Research, Korea Polar Research Institute, Incheon 406-840, South Korea

<sup>c</sup> Alfred Wegener Institute for Polar and Marine Research, Bremerhaven, Germany

## ARTICLE INFO

### Article history:

Received 30 August 2012

Received in revised form

14 March 2013

Accepted 16 March 2013

Editor: G. Henderson

Available online 25 April 2013

### Keywords:

<sup>143</sup>Nd/<sup>144</sup>Nd

Mendeleev Ridge

circulation

paleoclimate

ice-dammed lake

## ABSTRACT

The freshwater budget of the Arctic Ocean is a key component governing the deep water formation in the North Atlantic and the global climate system. We analyzed the isotopic composition of neodymium ( $\epsilon_{\text{Nd}}$ ) in authigenic phases of marine sediments on the Mendeleev Ridge in the western Arctic Ocean spanning an estimated time interval from present to about 75 ka BP. This continuous record was used to reconstruct the  $\epsilon_{\text{Nd}}$  of the polar deep water (PDW) and changes in freshwater sources to the PDW through time. Three deviations in  $\epsilon_{\text{Nd}}$  from a long term average of  $-10.2$  were identified at estimated 46–51, 35–39 and 13–21 ka BP. The estimated 46–51 ka BP event can be traced to bursting of ice-dammed lakes accompanying the collapse of the Barents–Kara Ice Sheet, which would have released radiogenic Nd to the eastern Arctic Ocean. The cyclonic surface circulation in the eastern Arctic Ocean must have been stronger than at present for the event to be recorded on the Mendeleev Ridge. For the 35–39 and 13–21 ka BP events, it is likely that the Laurentide Ice Sheet (LIS) supplied the unradiogenic freshwater. The configuration of the anticyclonic circulation in the western Arctic was probably similar to today or expanded eastward. Our simple mass balance calculations suggest that large amounts of freshwater were released but due to significant deep water formation within the Arctic Ocean, the effect on the formation of NADW was probably minor.

© 2013 Elsevier B.V. All rights reserved.

## 1. Introduction

In the modern Arctic Ocean, the primary freshwater sources are the riverine discharge, Pacific inflow through the Bering Strait and precipitation (Serreze et al., 2006). The largest sink is the flow into the North Atlantic through Fram Strait and Canadian Arctic Archipelago. The freshwater outflow from the Arctic Ocean may weaken the Atlantic meridional overturning circulation (Peterson et al., 2002; Tarasov and Peltier, 2005) and disrupt global climate. The Great Salinity Anomaly (1968–1982) (Dickson et al., 1988) is a recent example of a salinity depletion event in the North Atlantic caused by ice export from the Arctic Ocean (Aagaard and Carmack, 1989), and it possibly triggered the reduction of NADW in 1978–1982 (Schlosser et al., 1991). Therefore, reconstructing freshwater discharge events in the Arctic Ocean and tracing their origins are important for understanding paleoclimatic evolution and predicting future climate change.

To reconstruct past freshwater discharge events, light  $\delta^{18}\text{O}$  and  $\delta^{13}\text{C}$  values of planktonic foraminifera or occurrences of ice-rafted debris (IRD) have been used (Darby et al., 2006; Knies et al., 2007; Poore et al., 1999; Stein et al., 1994a, 1994b). Due to the semi-enclosed nature of the Arctic Ocean, low and stable Arctic surface water temperatures and diverse freshwater sources, the  $\delta^{18}\text{O}$  distribution of its surface waters reflects regional salinity variations rather than global temperature or ice volume changes (Spielhagen and Erlenkeuser, 1994; Stein et al., 1994b). Although the full picture is more complicated,  $\delta^{13}\text{C}$  depletion, if accompanied by  $\delta^{18}\text{O}$  reduction, is also interpreted as stratified and less productive surface waters (Poore et al., 1999). However,  $\delta^{18}\text{O}$  and  $\delta^{13}\text{C}$  values cannot pinpoint the source of the freshwater, and their variability can be muted in areas of low sedimentation rate because of the short residence time ( $\sim 10$ – $30$  yr) of the Arctic surface waters (Macdonald and Bowers, 1996). The abrupt increase in IRD accompanies collapsing ice sheets (Darby et al., 2006) but probably not outburst of ice dammed lakes from distal areas.

Neodymium (Nd) isotope ratios, expressed as  $\epsilon_{\text{Nd}} = \left[ \frac{(^{143}\text{Nd}/^{144}\text{Nd})_{\text{sample}}}{(^{143}\text{Nd}/^{144}\text{Nd})_{\text{CHUR}}} - 1 \right] \times 10^4$ , where  $(^{143}\text{Nd}/^{144}\text{Nd})_{\text{CHUR}}$  is 0.512638 (Jacobsen and Wasserburg, 1980), can be

\* Corresponding author. Tel.: +82 2880 9167; fax: +82 2871 8752.  
E-mail address: yuhuh@snu.ac.kr (Y. Huh).

a useful provenance proxy of freshwater discharge events to complement the stable isotope ratios and IRD. During partial melting of silicate minerals, the daughter element Nd preferentially partitions into the melt phase whereas the parent element Sm tends to stay in the residual solid (Faure and Mensing, 2005). Thus, old continental crust develops unradiogenic  $\epsilon_{Nd}$  values and young mantle rocks radiogenic values. The short residence time (200–1000 yr) of Nd in seawater (Tachikawa et al., 1999) allows the oceanic water masses to conserve the distinct  $\epsilon_{Nd}$  value of the source regions (e.g. Piotrowski et al., 2009; Rutberg et al., 2000). The  $\epsilon_{Nd}$  value of a water mass is in turn recorded in authigenic minerals such as the Fe–Mn oxyhydroxides which precipitate upon the surface of biogenic and detrital material from ambient water. Therefore, past variations in the water masses can be reconstructed through changes in  $\epsilon_{Nd}$  (e.g. Frank et al., 2002; Piotrowski et al., 2009; Rutberg et al., 2000; Spivack and Wasserburg, 1988). Here we analyzed authigenic Nd isotopes of

marine sediments from the Mendeleev Ridge in the Amerasian Basin of the Arctic Ocean at the depth of the Polar Deep Water (PDW) and reconstructed past  $\epsilon_{Nd}$  variations of and the contribution of freshwater to the PDW over the past ~75 kyr.

The water column of the Arctic Ocean is highly stratified, featuring the fresh Polar Mixed Layer at the surface, the cold Halocline Layer, the warm and saline Atlantic layer (AL) at approximately 200–850 m, the cooler and saltier Upper Polar Deep Water (UPDW) extending to 1700 m and the PDW (Porcelli et al., 2009). The average depth of the Lomonosov Ridge is ~1700 m and divides the PDW into the western Amerasian (subdivided into Canada and Makarov basins) and eastern Eurasian (subdivided into Amundsen and Nansen basins) basins (Fig. 1).

In general, the circulation in the PDW is not well known. Because of the higher temperature and salinity in the deep Arctic basins and the structure of increasing salinity with depth, slope convection has been inferred for the different basins of the Arctic

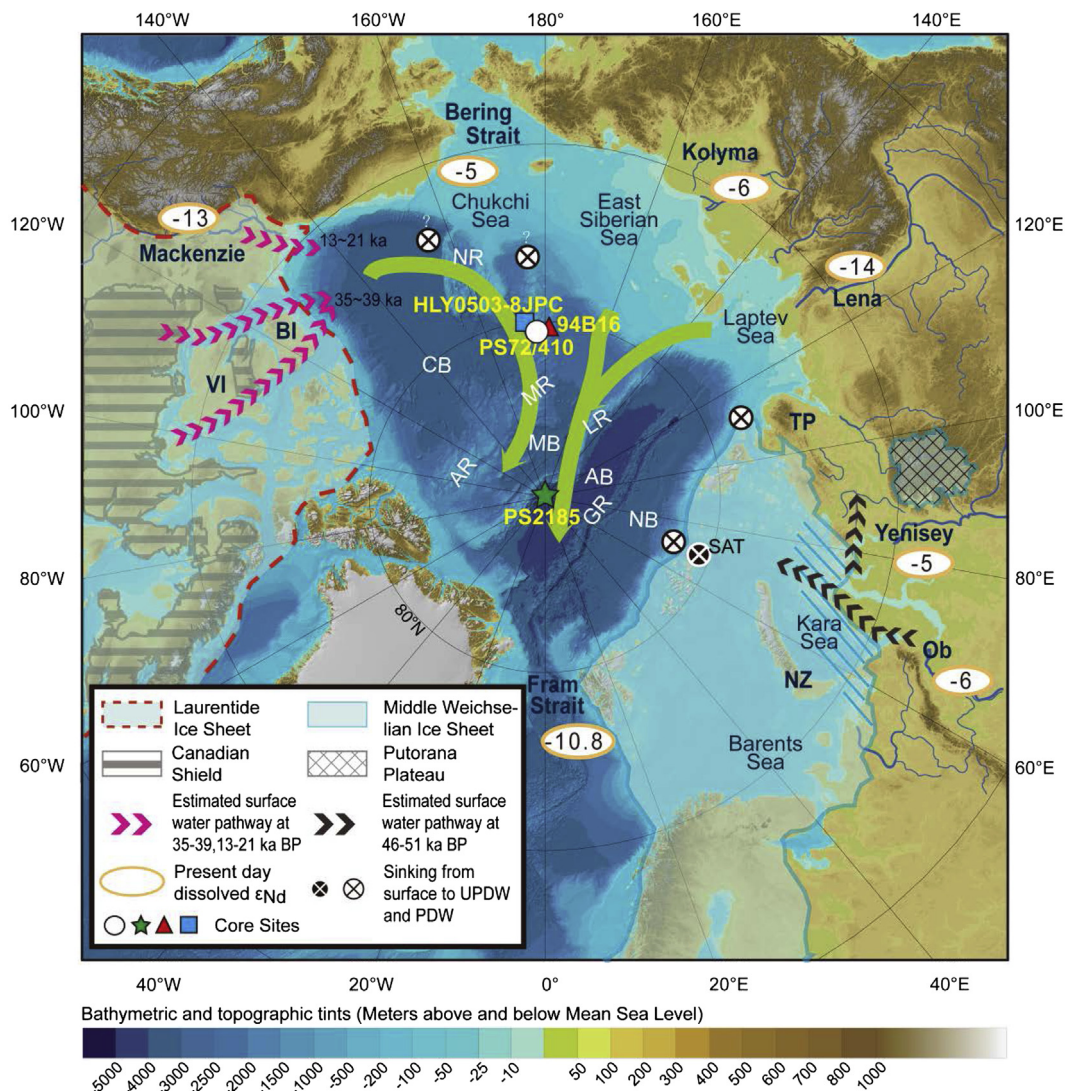


**Fig. 1.** Schematic map of the circum-Arctic showing core sites, ocean circulation and glacial ice sheet distribution. Yellowish green arrows mark the Beaufort Gyre and the Transpolar Drift. Sites are marked for core PS72/410 (white circle) and neighboring cores 94B16 (red triangle; Poore et al., 1999) and HLY0503-8JPC (blue square; Adler et al., 2009) on the Mendeleev Ridge and for core PS2185 (green star; Haley et al., 2007) on the Lomonosov Ridge. The  $\epsilon_{Nd}$  values of major inflows into the Arctic Ocean are given inside yellow ellipses (Porcelli et al., 2009 and references therein). The full glacial Laurentide Ice Sheet margin (dashed red line) and the Barents–Kara Ice Sheet margin at 60 ka BP (blue line) are simplified from Svendsen et al. (2004) and Stokes and Clark (2003), respectively. Note that the Putorana Plateau was under ice in the Middle Weichselian. Estimated surface water inflows during different periods are shown with purple and dark gray arrows. AB: Amundsen Basin, AR: Alpha Ridge, BI: Banks Island, CB: Canada Basin, GR: Gakkel Ridge, MB: Makarov Basin, MR: Mendeleev Ridge, NB: Nansen Basin, NR: Northwind Ridge, NZ: Novaya Zemlya, SAT: St. Anna Trough, TP: Taimyr Peninsula and VI: Victoria Island. The base map is IBCAO-3 from Jakobsson et al. (2012). (For interpretation of the references to color in this figure legend, the reader is referred to the web version of this article.)

Ocean (reviewed in Rudels et al. (2012)). In the Eurasian Basin, the cold and dense water formed in the Barents Sea sinking down the St. Anna Trough and deep water inflow through the Fram Strait contribute. However, in the Amerasian Basin no significant continuous flow from the Amundsen Basin across the central Lomonosov Ridge is observed (Björk et al., 2007). This implies that the PDW in the Amerasian Basin may be derived predominantly from density flow on the shelf.

The modern Nd isotopic composition of the water column also sheds some light on the source of PDW in the different Arctic basins. The present-day  $\epsilon_{\text{Nd}}$  values of potential source regions surrounding the Arctic Ocean are (i) the unradiogenic Atlantic water (−10.8) and the Mackenzie (−13) and Lena (−14) rivers and (ii) the radiogenic Pacific water (−5) and the Kolyma (−6), Ob (−6) and Yenisey (−5) rivers (data from Porcelli et al. (2009) and references therein). The AL displays significant differences in dissolved  $\epsilon_{\text{Nd}}$  in the three sub-basins (−9.6 and −9.1 for Canada, −10.9 for Makarov, and −11.6 for Admundsen basins; precision  $\pm 0.4$ ) indicating involvement of waters that have been modified by shelf–water interaction (Porcelli et al., 2009). The  $\epsilon_{\text{Nd}}$  values are dominated by the Atlantic signal throughout the deep Arctic Ocean, but there are discernible local variations. The  $\epsilon_{\text{Nd}}$  of PDW of the Canada Basin interior (−11.0) is similar to that of the Makarov Basin (−10.5, −10.7) but different from that of the Amundsen Basin (−12.3). This suggests local convection within the Amerasian basin entraining basin-specific AL during convection. The PDW of the Canada Basin near the slope has a more radiogenic value (−9.0) than in the interior or other basins (Porcelli et al., 2009). This may indicate slope convection entraining the radiogenic Pacific water and provides a clue as to where slope convection is occurring. Such slope convection would have been more practical during freshwater discharge events, when sea-ice and brine formation would have been enhanced (e.g. Dokken and Jansen, 1999; Risebrobakken et al., 2006) and sediment-loaded meltwater may have formed hyperpycnal flows (e.g. Aharon, 2006). Thus, we hypothesize that abrupt variations in the quantity and composition of the surface water can, through slope convection, affect the  $\epsilon_{\text{Nd}}$  of the PDW, and we aim to trace the freshwater discharge events from its paleoceanographic record.

## 2. Method

### 2.1. Sampling location

Sediment core samples were obtained at site PS72/410 (80°30.37'N, 175°44.38'W, 1808 m water depth) on the central part of the Mendeleev Ridge in the western Arctic Ocean during RV *Polarstern* Expedition ARK-23/3 in 2008 (Fig. 1). The 39 cm-long sediment core 410-1 was taken using the Giant Box Corer and sampled onboard at 1 cm resolution. Present-day surface water circulation at the site is governed by the Beaufort Gyre, and the freshwater inputs are mainly from the Pacific and the Mackenzie River with variable influence of the Eastern Siberian rivers depending on the local wind pattern (Alkire et al., 2010; Guay et al., 2001; Macdonald et al., 2000) (Fig. 1).

### 2.2. Nd isotope analysis

#### 2.2.1. Fe–Mn oxyhydroxide extraction

The sequential chemical extraction steps were modified from Bayon et al. (2002), Chester and Hughes (1967) and Gutjahr et al. (2007). Approximately 1 g of ground sediment was repeatedly (for most samples twice) treated with 1 M buffered acetic acid (pH ~5) until carbonates were thoroughly removed. The Fe–Mn oxyhydroxide

fraction was retrieved from the decarbonated sediment using 14 ml 0.02 M hydroxylamine hydrochloride in 25% acetic acid buffered to pH ~4 for 3 h at room temperature. Although this mild leaching technique may not extract all the Fe–Mn oxyhydroxide, it prevents contamination by detrital phases. After adding 1 ml of concentrated  $\text{HNO}_3$  in order to remove excess reducing agent, the sample was evaporated to dryness and dissolved in 0.5 ml of 2 M  $\text{HNO}_3$  for column separation.

#### 2.2.2. Column chemistry

The column separation method was based on Míková and Denková (2007) and Pin and Zalduegui (1997). TRU resin (50–100  $\mu\text{m}$ , Eichrom) packed to 0.25 ml bed volume in Bio-rad Poly-Prep chromatography columns (0.8 cm ID, 5 cm long, 10 ml reservoir) was used to separate LREEs from the extracted Fe–Mn oxyhydroxide fraction. Columns were washed with 8 ml of ultrapure-water and pre-conditioned with 6 ml of 2 M  $\text{HNO}_3$ . After sample loading, the fraction containing Sr, Fe, Ca and HREEs was eluted with 8 ml of 2 M  $\text{HNO}_3$ . LREEs including Nd were recovered using 6 ml of 0.05 M HCl. The TRU resin was not reused. For samples with high cation concentrations, cation exchange resin (AG50W-X8, 100–200 mesh) separation was carried out prior to the TRU resin step.

The Ln resin (50–100  $\mu\text{m}$ , Eichrom) was packed to 0.7 ml bed volume in Teflon columns. The LREE fraction was loaded and the matrix containing La, Ce and Pr was eluted with 2 ml of 0.25 M HCl. The Nd fraction was collected with 5 ml of 0.25 M HCl. The Ln resin did not pose Nd blank problems; the resin was reused and the elution calibration was periodically checked (Míková and Denková, 2007).

#### 2.2.3. TIMS analysis

Nd isotopes were analyzed using thermal ionization mass spectrometer (IsoProbe-T, IsotopX) at the Korea Basic Science Institute. Interference correction was carried out with  $^{147}\text{Sm}/^{146}\text{Nd}$ , and mass fractionation correction was made by normalizing  $^{146}\text{Nd}/^{144}\text{Nd}$  to 0.7219. During the course of this study, JNdi-1 standard had an average  $^{143}\text{Nd}/^{144}\text{Nd}$  of 0.512098. External reproducibility of replicate analyses of JNdi-1 was  $\pm 0.000011$  ( $2\sigma$ ,  $n=30$ ) on  $^{143}\text{Nd}/^{144}\text{Nd}$  and  $\pm 0.2$  in the  $\epsilon$  units (Supplementary Table S1).

### 2.3. Geochemical and sedimentological data

Oxygen and carbon isotope ratios of planktonic foraminifera (*Neoglobobulimina pachyderma* sin.) in the > 125 mm fraction were measured using Finnigan MAT 252 at Alfred Wegener Institute. The mass spectrometer (Finnigan MAT252 with automated carbonate preparation device Kiel Carbo) was calibrated via international standard NBS19 to the PDB scale, and results are given in  $\delta$ -notation versus Vienna PDB. The precision of  $\delta^{18}\text{O}$  and  $\delta^{13}\text{C}$  measurements, based on an internal laboratory standard (Solnhofen limestone) measured over a 1 yr period together with samples, was better than  $\pm 0.08\text{‰}$  and  $\pm 0.06\text{‰}$ , respectively. Bulk carbon and total organic carbon were measured using a CHN analyzer at University of Kiel, and inorganic carbon contents were calculated by difference between these values. As the inorganic carbon may be related to unknown proportions of calcite or dolomite (cf., Stein et al., 2010), we have not transferred the inorganic carbon values into carbonate percentages.

The  $L^*$  (lightness, black (0) to white (100)) and  $a^*$  (red–green color space, green (−4) to red (16)) values were determined on a 38 cm-long subcore using the Minolta spectrophotometer (lens diameter 8 mm, field of view  $\varnothing$  0.8 cm) at wavelengths from 400 to 700 nm (Jokat, 2009). In the same subcore, gravel particles (> 2 mm) were counted at 1 cm interval across the x-ray slab in a field of  $10 \times 1 \times 1 \text{ cm}^3$  and reported as IRD (see more Matthiessen

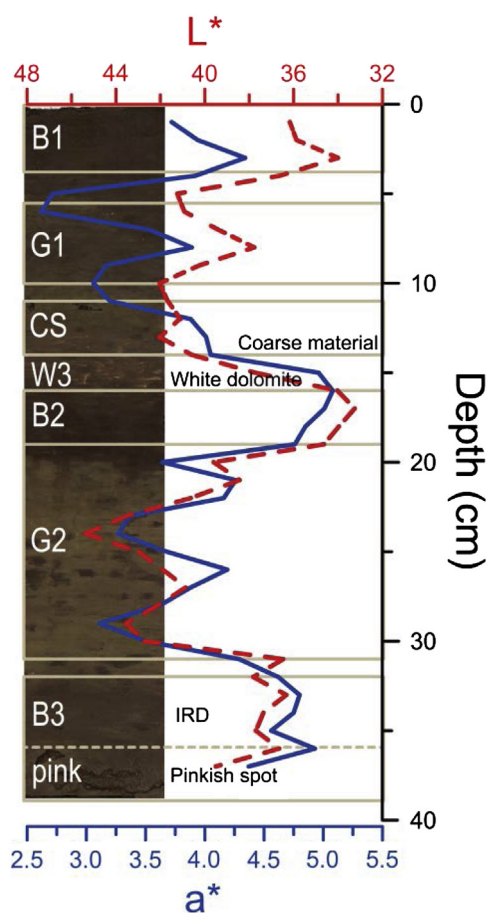


**Fig. 2.** Sediment stratigraphy based on the line-scan image and  $L^*$  (dashed red line) and  $a^*$  values (blue line). Brown (B) and Gray (G) layers were assigned based on grain size and sediment color— $L^*$  and  $a^*$  values. The accurate position of the W3 and pinkish dolomite layer are uncertain due to widely scattered dolomite spots observed on the line-scan image. CS stands for condensed section. (For interpretation of the references to color in this figure legend, the reader is referred to the web version of this article.)

et al., 2010). Line-scan digital core images were taken with the Avaatech digital imaging system (Fig. 2). All data are stored in the databank PANGAEA (<http://www.pangaea.de>).

### 3. Results and discussion

#### 3.1. Core information

The core is mainly composed of sandy-silty clay of brown to dark brown, dark yellowish brown, olive to olive brown and dark grayish brown colors (Jokat, 2009; Stein et al., 2010) (Fig. 2). The surface is dark brown sandy mud with many dropstones ( $\varnothing$  up to 2 cm) (Jokat, 2009). A cyclic alternation of brown and gray sediment is observed, which is probably caused by variations in manganese concentrations. Such pattern is generally used as an indicator of interglacial (interstadial, high Mn) and glacial (stadial, low Mn) conditions (Jakobsson et al., 2000). We classified the sediment layers based on grain size and sediment color— $L^*$  (black to white) and  $a^*$  (green to red) values (Fig. 2). These criteria have been used widely in Arctic sediments to construct stratigraphic sequence (Adler et al., 2009; Darby et al., 2006; Polyak et al., 2004, 2009). The brown layer 1 (B1, 0–4 cm) is characterized by dark brown sandy silty clay with relatively low  $L^*$  and high  $a^*$  values. The gray layer 1 (G1, 5.5–10 cm) is designated based on shipboard core description (Stein et al., 2010). It is mainly composed of dark grayish brown clay to very dark grayish brown

sandy silty clay. We labeled the 11–14 cm interval of mainly brown (sandy) silty clay a condensed section (CS) (see Section 3.2 age model) (Fig. 2). It overlies a thin layer of coarse material which was also observed in neighboring cores 94B16 (80°20.33'N, 178°42.71'W; Poore et al. (1999)) and HLY0503-8JPC (79°35.6'N, 172°30.1'W; Adler et al. (2009)) on the Mendeleev Ridge. The 10–11 cm depth interval is olive silty clay and its characteristic color and grain size are clearly distinct from the CS. The B2 layer (14–19 cm) consists of brown, dark brown and dark yellowish brown silty clay with variable degrees of bioturbation. It has low  $L^*$  and high  $a^*$  values. White dolomite lenses and spots observed toward the top of the B2 layer is designated as the white layer W3 (14–16 cm) (Stein et al., 2010). This layer is common to the three neighboring Mendeleev Ridge cores (Adler et al., 2009; Polyak et al., 2004, 2009), and we used it as a consistency check for our age model. Dolomite has generally been considered to derive from the Canadian Arctic Archipelago, especially from the Banks and Victoria islands (Adler et al., 2009; Stein et al., 2010). The G2 layer (19–31 cm) contains dark grayish brown and olive brown silty clay. The B3 layer (32–39 cm) is similar to the B2 layer except for the larger grain size. In particular, a prominent IRD peak is observed at 34 cm. Some 'pinkish' dolomite spots indicating the Banks and Victoria islands source were identified (36–39 cm), which is also consistent with previous descriptions of the B3 layer in other Mendeleev Ridge cores (Adler et al., 2009; Stein et al., 2010).

#### 3.2. Age model

It is difficult to construct age models for Arctic Ocean sediments because of the low sedimentation rate and limited biotic remains (Polyak et al., 2004). In recent years, several studies have used stratigraphic approaches that bring together different proxies such as grain size, manganese content, total planktonic and benthic foraminiferal abundances, calcareous nannofossil abundances, lithology,  $L^*$  and  $\delta^{18}\text{O}$  and  $\delta^{13}\text{C}$  of planktonic foraminifera under the assumption that these proxy variations reflect climate cyclicity (Adler et al., 2009; Backman et al., 2009; Darby et al., 2006; Polyak et al., 2004). We used AMS  $^{14}\text{C}$  ages ( $n=6$ ) and correlated our planktonic  $\delta^{18}\text{O}$  and  $\delta^{13}\text{C}$ ,  $L^*$  and sediment lithology with cores 94B16 and HLY0503-8JPC on the Mendeleev Ridge (Fig. 3).

AMS  $^{14}\text{C}$  ages were obtained for planktonic foraminifera (*N. pachyderma* sin.) at depth intervals 1–2, 10–11, 13–14 and 20–21 cm at Leibniz Laboratory, Kiel and at depth intervals 8–9 and 11–12 cm at Center for Applied Isotope Studies, Georgia. They were converted to calendar years using Marine09 (Reimer et al., 2009) to ca. 5.1, 19.8, 30.8 and 46 ka BP and 9.1 and 20.6 BP, respectively (Supplementary Table S2). A regional difference of reservoir effect ( $\Delta R=1000$ ) was assumed (Hanslik et al., 2010). We recalculated the AMS  $^{14}\text{C}$  ages of cores 94B16, HLY0503-8JPC and PS2185 for consistency (Supplementary Table S2).

We correlated lithostratigraphic sequences including brown layers B1–B3 and white layer W3 (Fig. 3). The base of B1 is 6.5 ka BP by interpolation between the two youngest AMS ages, which is slightly younger than in the other cores. It is possibly due to too few control points for the Holocene of our core. The higher sedimentation rate in the Arctic area during the early versus late Holocene (Keigwin et al., 2006) can explain the uncertainty in interpolation and the younger age of the base of B1 for PS72/410-1. Therefore, we followed previous stratigraphic age (8.1 ka BP), which is supported by the stable isotope correlation (Fig. 3). The AMS ages of 46 ka BP at 20.5 cm slightly below the base of B2 in PS72/410-1, 45 ka at 26.5 cm in the B2 layer of 94B16 and 41 and 43 ka BP at 56.5 cm and 62.5 cm in the B2 layer of HLY0503-8JPC agree fairly well. The age of the B3 layer is more tentative. According to Adler et al. (2009), B3 coincides with the top of MIS5 (~75 ka BP) whereas Backman et al. (2009) correlate B3 with the base of MIS3 (~60 ka BP) (Fig. 4; see Stein et al. (2010) for further

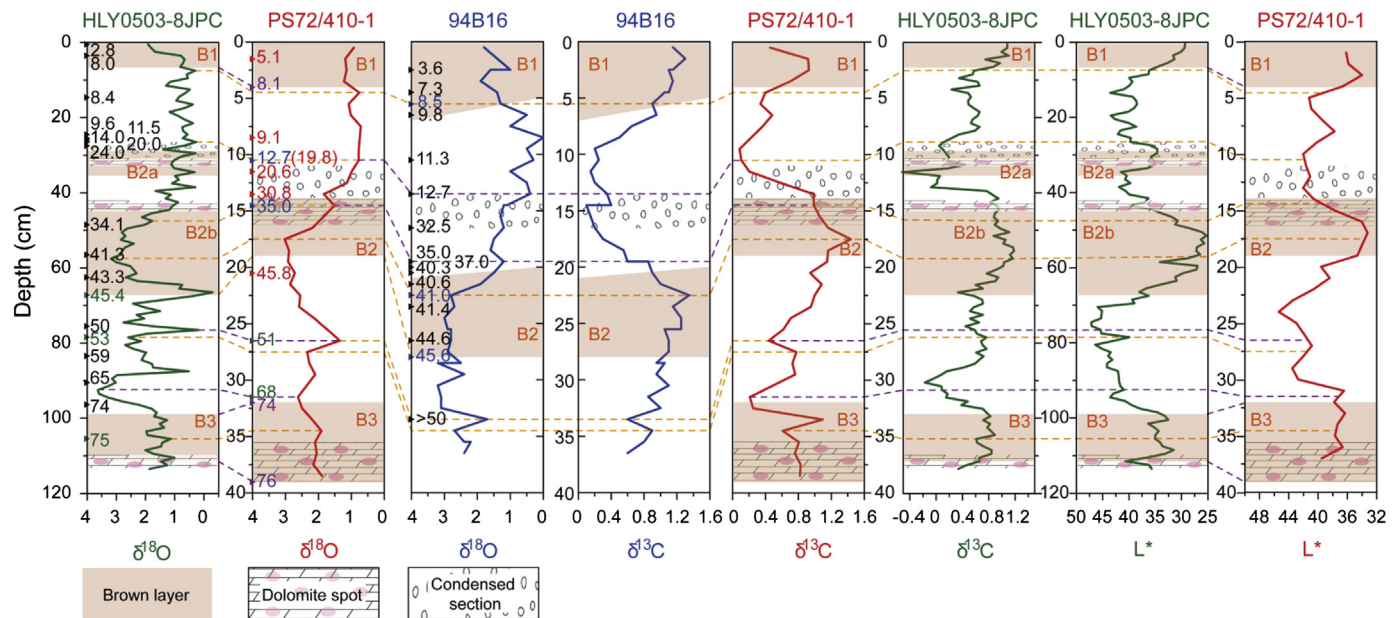


**Fig. 3.** Age model construction for core PS72/410-1 using AMS  $^{14}\text{C}$  ages (ka BP,  $n=6$ , red numbers) and by correlating  $\delta^{18}\text{O}$ ,  $\delta^{13}\text{C}$  and  $L^*$  (red lines) with neighboring cores 94B16 (blue lines; Poore et al., 1999) and HLY0503-8JPC (green lines; Adler et al., 2009) for which stratigraphic ages have already been constructed. The numbers (ka BP) in the  $\delta^{18}\text{O}$  graph of PS72/410-1 represent AMS  $^{14}\text{C}$  ages (red), stable isotope correlation ages with cores 94B16 (blue) and HLY0503-8JPC (green) and stratigraphic ages (purple) that are used as age control points. The numbers (ka BP) in the  $\delta^{18}\text{O}$  graph of 94B16 and HLY0503-8JPC indicate age control points of the original authors including AMS  $^{14}\text{C}$  ages (ka BP). The ages of tie points matched to cores 94B16 and HLY0503-8JPC are shown in the green and blue numbers (ka BP) of the  $\delta^{18}\text{O}$  graph of each core. Purple dashed lines link the age control points and orange dashed lines mark other tie points. Characteristic sediment layers are shown with patterned rectangles. (For interpretation of the references to color in this figure legend, the reader is referred to the web version of this article.)

discussion). Using planktonic  $\delta^{18}\text{O}$  and  $\delta^{13}\text{C}$  values as well as  $L^*$  values for correlation between cores HLY0503-8JPC and PS72/410-1 and following the age model of Adler et al. (2009), we propose a tentative age of about 74 ka for the top and base, respectively, of the B3 layer in core PS72/410-1. The age of the W3 layer at 14–16 cm is comparable to those determined in other Mendeleev Ridge cores.

Based on the calibrated  $^{14}\text{C}$  ages for cores 94B16 and HLY0503-8JPC and  $L^*$  and sediment color for HLY0503-8JPC, we matched  $\delta^{18}\text{O}$  and  $\delta^{13}\text{C}$  of planktonic foraminifera (*N. pachyderma* sin.) for stratigraphic correlation. Six  $\delta^{18}\text{O}$  and  $\delta^{13}\text{C}$  tie points were matched to core 94B16 and eight to HLY0503-8JPC, among which four were selected to be age control points as explained below (Fig. 3). The first pair of age control points was in the CS layer where sedimentation rates were strongly reduced. Similar features have been interpreted as either a hiatus (Polyak et al., 2009) or as removal by contour currents of sediments deposited during Marine Isotope Stage (MIS) 2 (Poore et al., 1999). The x-radiograph (shown in Matthiessen and Stein (2008)) does not show an unconformity yet the layer is bioturbated, leaving open the possibility that a hiatus was erased. The CS is bracketed by AMS ages in 94B16 and has an AMS age at its base in PS72/410-1, and in core HLY0503-8JPC the top of the CS is interpolated to an age of 13 ka BP. Thus, considering all three cores, the age of the CS broadly lasted from 30.8 ka BP to 12.7 ka BP. The low stable isotope values were special features at the termination depth of CS in the three neighboring cores. The AMS  $^{14}\text{C}$  age for termination of the CS in core PS72/410-1 (19.8 ka BP at 10.5 cm) (Supplementary Table S2) is older than the 12.7 ka BP and is probably due to a bias in  $^{14}\text{C}$  age toward older values by meltwater derived from old carbonate rocks in northwest Canada (cf., Polyak et al., 2009) or by poor preservation in the CS of young foraminifera by loss of saline habitat during deglaciation. The second pair of age control points is from the correlation with core HLY0503-8JPC. The light  $\delta^{18}\text{O}$  and  $\delta^{13}\text{C}$  at 26.5 cm depth in PS72/410-1 were observed at > 50 ka in core 94B16 and at 51 ka BP in core HLY0503-8JPC. The heavy  $\delta^{18}\text{O}$  and light  $\delta^{13}\text{C}$  at 31.5 cm depth in PS72/410-1 was also a prominent feature in core HLY0503-8JPC (Adler et al., 2009).

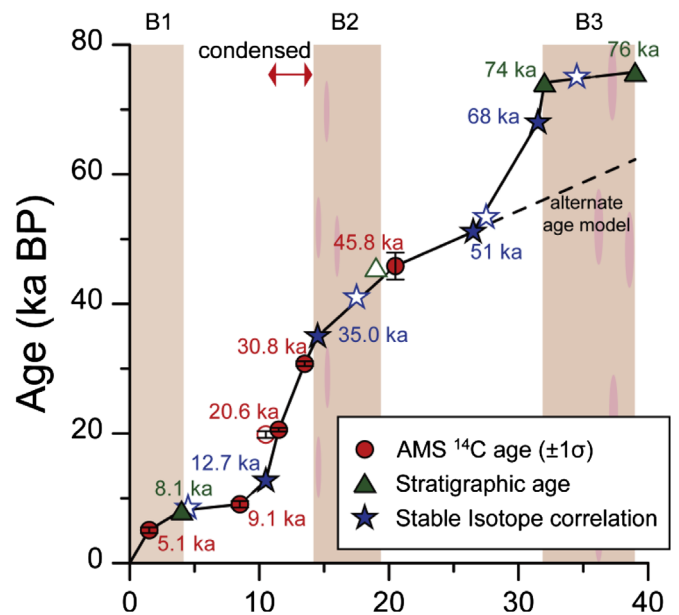


**Fig. 4.** Proposed age model for core PS72/410-1 (based on AMS  $^{14}\text{C}$  datings and correlation with core HLY0503-8JPC; Adler et al., 2009). Closed symbols with black outlines indicate age control points including the five AMS  $^{14}\text{C}$  ages, three lithostratigraphic correlation ages and four stable isotope correlation ages. Open symbols represent stable isotope and  $L^*$ , lithostratigraphic tie points and an apparently contaminated AMS  $^{14}\text{C}$  age. In addition, an alternate age model based on Backman et al. (2009) is presented for the lower part of the record (dashed line; Stein et al., 2010 for further discussion). The vertical brown bars indicate brown layers, and the red arrow represents the condensed section. (For interpretation of the references to color in this figure legend, the reader is referred to the web version of this article.)

In summary, we used five calibrated AMS  $^{14}\text{C}$  ages, four stable isotope correlation ages (two from 94B16 and two from HLY0503-8JPC) and three lithostratigraphic correlation ages (the termination of the B1 layer and the initiation and termination of the B3

layer) as age control points. According to our preferred, still tentative age model for PS72/410-1 which extends to MIS 5a (Fig. 4), the sedimentation rates during interstadial periods were generally higher than during stadial periods.

### 3.3. Nd isotopes

The core top  $\epsilon_{\text{Nd}}$  was  $-10.6 \pm 0.2$  ( $2\sigma$ ) which is similar to the present-day water column in the Canada Basin at 1000 and 3000 m depths (Porcelli et al., 2009) (Fig. 5). The average  $\epsilon_{\text{Nd}}$  ( $n=39$ ) throughout the sampled stratigraphic interval was

$-10.2 \pm 1.7$  ( $2\sigma$ ), similar to the core top value, from which three periods of significant  $\epsilon_{\text{Nd}}$  deviations occurred (Fig. 5).

#### 3.3.1. Radiogenic $\epsilon_{\text{Nd}}$ peak at estimated 46–51 ka BP

A pronounced  $\epsilon_{\text{Nd}}$  high was observed in the upper part of G2. It immediately followed minima in  $\delta^{18}\text{O}$  and  $\delta^{13}\text{C}$  of planktonic foraminifera at 51 ka BP (Fig. 5) which indicate a large episodic input of freshwater. Then, it appears that there is a minimum and a slight maximum again in  $\epsilon_{\text{Nd}}$  that is accompanied by only slight minima in  $\delta^{18}\text{O}$  and  $\delta^{13}\text{C}$ . This second freshwater peak is more prominent in core HLY0503-8JPC which has about three times higher sedimentation rate than PS72/410-1 (Fig. 3) and could very

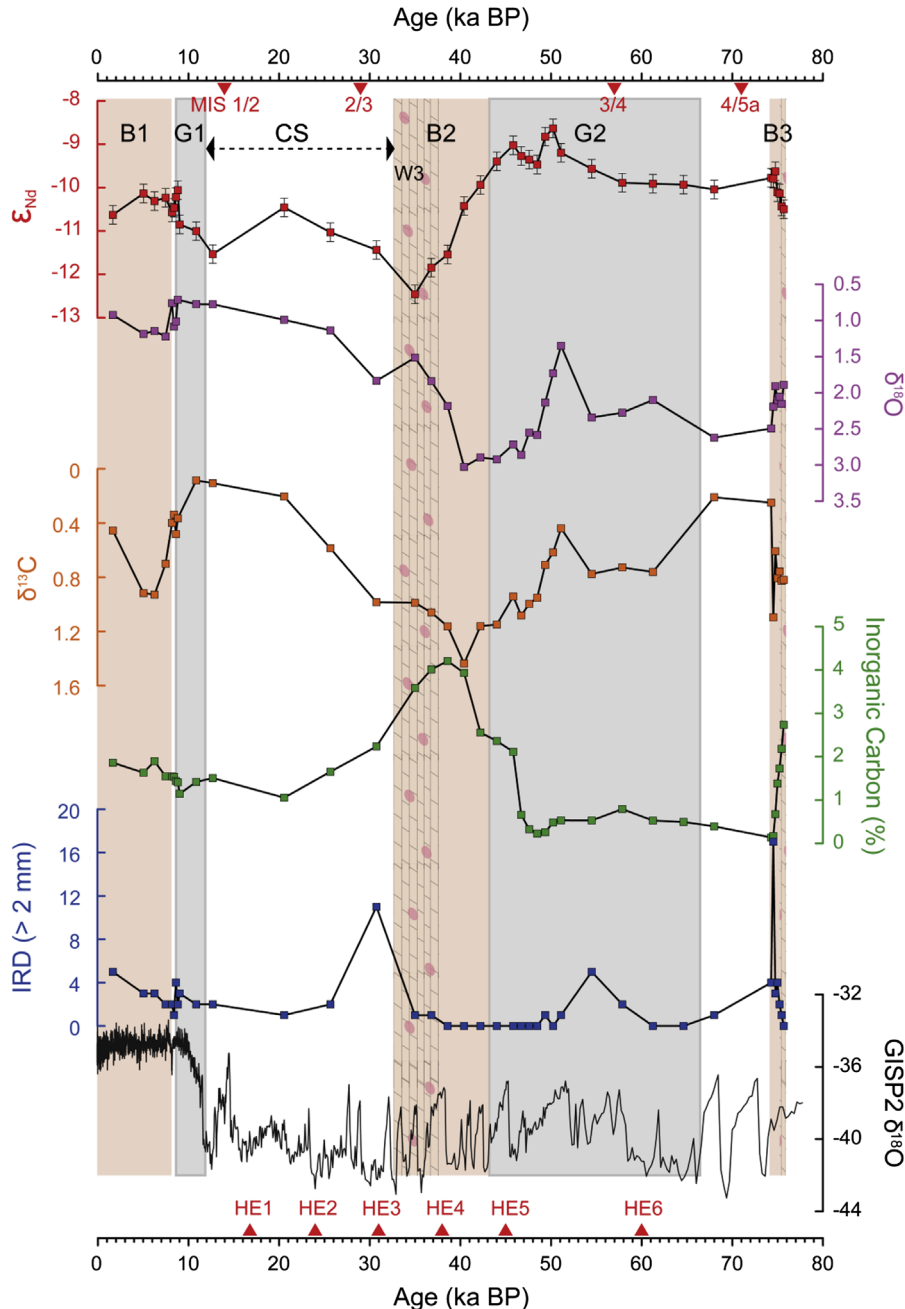


**Fig. 5.** Proxy data for core PS72/410-1, plotted vs. age (for age model see Fig. 4). Nd isotope data show three prominent  $\epsilon_{\text{Nd}}$  deviations from the average ( $-10.2 \pm 1.7$ ).  $\epsilon_{\text{Nd}} = [(^{143}\text{Nd}/^{144}\text{Nd})_{\text{sample}} / (^{143}\text{Nd}/^{144}\text{Nd})_{\text{CHUR}} - 1] \times 10^4$ . Error bars on  $\epsilon_{\text{Nd}}$  indicate  $\pm 2\sigma$  external uncertainties ( $0.2\epsilon_{\text{Nd}}$  units). Coarse-grained ( $> 2$  mm) ice-rafted debris counts, inorganic carbon content and  $\delta^{18}\text{O}$  and  $\delta^{13}\text{C}$  of planktonic foraminifera (*N. pachyderma* sin.) in PS72/410-1 are also illustrated for comparison as is GISP2  $\delta^{18}\text{O}$  values (Grootes and Stuiver, 1999). The ages of Heinrich events are marked with red triangles (Hemming, 2004) and marine isotope stages with inverted triangles (Lisiecki and Raymo, 2005). Vertical bars denote characteristic sediment layers—brown: B layers, gray: G layers, pattern with pink spots: dolomite layers. The condensed section (CS) is marked with a dashed horizontal arrow. (For interpretation of the references to color in this figure legend, the reader is referred to the web version of this article.)

well be related to another freshwater discharge event to the Arctic. As the second peak is rather tentative, we will not discuss this further at this time.

The source of the freshwater for the first peak can be constrained, based on the radiogenic  $\epsilon_{\text{Nd}}$  value, to either the Pacific inflow or the Siberian rivers (the Kolyma, Yenisey and Ob) (Fig. 1). The only gateway to the Pacific, the Bering Strait, is narrow (~85 km) and shallow (~50 m) and hence almost closed at ~50 ka BP (Hu et al., 2010). Therefore, we can rule out the Pacific inflow. The present-day Nd fluxes from the Yenisey and Ob rivers into the Arctic Ocean (the PARTNERS project (<http://arcticgreatrivers.org/data.php>)) for Nd concentrations and Milliman and Farnsworth (2011) for mean annual discharge) are ~7 times greater than that from the Kolyma River (Supplementary Table S3), and there is indeed inference of freshwater discharge in the Yenisey–Ob region at ~50 ka BP. During the Middle Weichselian (60–50 ka BP), the ice sheet expanded from the Barents and Kara sea shelves to mainland Russia including west Siberia (Svendsen et al., 2004), blocked northward riverine discharge of Yenisey and Ob rivers and formed ice dammed lakes in northern Eurasia (Mangerud et al., 2004). The proglacial lake volume is estimated to have been 50,000 km<sup>3</sup>, about 50 times the annual discharge of the Yenisey and Ob rivers (Mangerud et al., 2004). Furthermore, weathering of basalts from the Putorana Plateau ( $\epsilon_{\text{Nd}} \sim 2$  from Sharma et al. (1992)) under the ice sheet could have intensified the supply of radiogenic Nd to the ice-dammed lakes (Fig. 1).

For the radiogenic  $\epsilon_{\text{Nd}}$  signals from the west Siberian shelf to be recorded on the Mendeleev Ridge, the cyclonic surface water circulation in the eastern Arctic must have extended further into the Canada Basin and fed the PDW by brine formation. Direct input into the PDW of the Eurasian Basin by hyperpycnal flow would not reach the Canada Basin due to blockage by the Lomonosov Ridge. Such extended cyclonic surface water circulation pattern has been inferred for the past 8000 yr based on matching the source of ice-rafted Fe grains in the Arctic (Darby et al., 2012) and for the last 155 kyr based on changes in the organic matter and carbonate content of sediments (Rella and Uchida, 2011). These studies attributed the phenomena to the change of sea level atmospheric pressure as in the case of Arctic Oscillation which governs the present-day surface water circulation in the Arctic (Morison et al., 2012). Another possible mechanism initiating the change in surface ocean circulation is the rise of the dynamic ocean topography (DOT) in the eastern Arctic triggered by outburst of ice-dammed lakes (Hu et al., 2012). Even though the underlying cause of the circulation change is highly speculative, the strong cyclonic surface current at estimated 46–51 ka BP seems to have transported eastern Arctic freshwater to western Arctic.

A cyclonic surface water circulation pattern was observed in 2008 from which we can draw some inferences. According to a mass balance calculation using total alkalinity, the inflow of Eurasian runoff into the southern Canada Basin was calculated to be more than 4.5 times the Mackenzie runoff (Alkire et al., 2010). Using the mean annual discharge of the Mackenzie River of ~310 km<sup>3</sup>/yr (Milliman and Farnsworth, 2011), it is estimated that ~1400 km<sup>3</sup>/yr of Eurasian river discharge flowed into the western Arctic. This is about half of total Eurasian river runoff. Extrapolating this, we assumed that at estimated 46–51 ka BP also, about half of the proglacial lake volume (25,000 km<sup>3</sup>) was incorporated into the western Arctic surface waters (Fig. 8).

### 3.3.2. Unradiogenic $\epsilon_{\text{Nd}}$ peaks at estimated 35–39 ka BP and 13–21 ka BP

Prominent  $\epsilon_{\text{Nd}}$  lows were observed in W3 and at the top of the CS (Fig. 5), and the unradiogenic Nd can be traced to the Canadian Shield or the Aldan Shield in Siberia presently drained by the Lena

River (Fig. 1). The stable isotope ratios decreased during these time intervals though not always recording minima (Fig. 5). The muted  $\delta^{18}\text{O}$  and  $\delta^{13}\text{C}$  signals may be due to the lower sedimentation rates than for the 46–51 ka BP event (1/6 during 35–39 and 1/2 during 13–21 ka BP) which smooth out rapid changes in the surface water.

During the 35–39 ka BP period, inorganic carbon contents were high (Fig. 5), which points to the extensive Paleozoic platform carbonate in northern Canada (Phillips and Grantz, 2001 and references therein) rather than the catchment of the Lena River. White dolomite attributed to the Banks and Victoria islands origin (Stein et al., 2010) was also observed in this section (Jokat, 2009). We infer that abrupt meltwater discharge from the waning LIS on the Precambrian Canadian Shield toward the Canadian Archipelago was responsible for the 35–39 ka BP event. For this signal to be recorded at our site, the general configuration of the Beaufort Gyre must have been similar to today or perhaps expanded toward the eastern Arctic by enhanced DOT in the western Arctic. High mechanical erosion under the LIS may have accumulated weathering products containing unradiogenic Nd on the exposed shelves, and when the LIS disintegrated and sea level rose, this material could have interacted with the meltwater to release unradiogenic Nd to Arctic surface waters. The estimated time interval for this event has large uncertainties and can accommodate the Heinrich event (HE) 4 at 38 ka BP (Hemming, 2004).

During the 13–21 ka BP period, the inorganic carbon content was comparable to present-day levels (Fig. 5), and no dolomitic layer was reported (Jokat, 2009). Considering only the timing, this event may be related to either the HE 1 at 16.8 ka BP (Hemming, 2004) also documented as an Arctic IRD event AL2 (Darby et al., 2002) or the outburst of glacial Lake Agassiz to the Arctic through the Mackenzie ice stream during the Younger Dryas (Fahl and Stein, 2012; Murton et al., 2010; Not and Hillaire-Marcel, 2012) (Fig. 1). The timing, source and pathway for the youngest event is open to debate due to uncertainties in the age model and to lack of  $\epsilon_{\text{Nd}}$  data points between 13 and 21 ka BP.

### 3.3.3. Comparison with the Lomonosov Ridge record

During slope convection to form the PDW, descending surface water can entrain significant amounts of water from the AL and the UPDW (Jones et al., 1995). Unlike the PDW, the AL and UPDW generated in the eastern Arctic Ocean are distributed to the western Arctic Ocean (Woodgate et al., 2001). In order to evaluate the influence of the UPDW, we compared our data with core PS2185 (87.5°N, 144.4°E, 1074 m water depth) on the Lomonosov Ridge

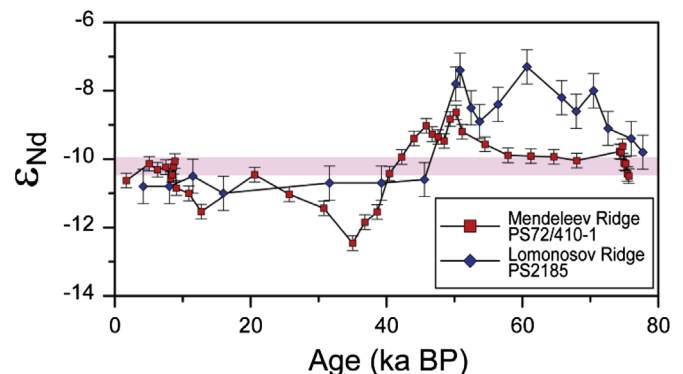


**Fig. 6.** Authigenic  $\epsilon_{\text{Nd}}$  records for the Polar Deep Water on the Canada Basin side of the Mendeleev Ridge (red square) and for the Upper Polar Deep Water on the Amundsen Basin side of the Lomonosov Ridge (blue diamond; Haley et al., 2007). The horizontal bar is the average  $\epsilon_{\text{Nd}}$  of core PS72/410-1. Error bars indicate  $\pm 2\sigma$  external uncertainties (0.2 $\epsilon_{\text{Nd}}$  units in PS72/410-1 and 0.5 $\epsilon_{\text{Nd}}$  units in PS2185). For age model see Fig. 4. (For interpretation of the references to color in this figure legend, the reader is referred to the web version of this article.)

(Haley et al., 2007) bathed by eastern Arctic waters (Figs. 1 and 6). The Lomonosov Ridge record is of lower resolution than our Mendeleev Ridge record, but the average  $\epsilon_{\text{Nd}}$  values are similar between the two and to the average AL value (Porcelli et al., 2009).

In the 55–76 ka BP period, radiogenic  $\epsilon_{\text{Nd}}$  is observed only in the Lomonosov Ridge record (Fig. 6). We infer that there was input of radiogenic Nd to surface waters which was localized to the eastern Arctic and fed the UPDW there, but the UPDW in the eastern Arctic was not a significant source for the PDW of the Canada Basin. At 46–51 ka BP, outburst of the ice-dammed lake changed the situation, and the surface waters of the eastern Arctic expanded to the west and affected its PDW. At this time, radiogenic  $\epsilon_{\text{Nd}}$  is observed in both records. At 30–40 ka BP, collapse of the LIS released unradiogenic Nd to the western Arctic surface waters but its influence was confined to the PDW of the western Arctic by the Beaufort Gyre. The unradiogenic  $\epsilon_{\text{Nd}}$  is only observed in the Mendeleev record.

### 3.3.4. Mass balance calculations

We carried out a simple mass balance calculation to estimate the amount of freshwater input that can explain the  $\epsilon_{\text{Nd}}$  excursions observed in the Mendeleev Ridge record. The many assumptions that we are obliged to make necessitates that this is only a crude guideline. For the PDW end member, we took the  $\epsilon_{\text{Nd}}$  value (−10.6) of the core top and present-day Nd concentration of PDW (16.7 pM from Porcelli et al. (2009)). The volume of PDW in the Amerasian Basin was assumed to be  $3.34 \times 10^6 \text{ km}^3$  based on the volume of water mass deeper than 1700 m in the central Arctic basin ( $\sim 5.27 \times 10^6 \text{ km}^3$  from Jakobsson et al. (2002)) weighted by the areas of sub-basins. The freshwater end member for the 46–51 ka BP was the Putoranan basalt ( $\epsilon_{\text{Nd}} = +2$  from Sharma et al. (1992)) and that for the 35–39 ka BP and 13–21 ka BP was the Canadian Shield ( $\epsilon_{\text{Nd}} = -24$  from Winter et al. (1997)) (Fig. 7). The Nd concentration for the radiogenic end member was assigned a value (700 pM) obtained from the average concentration and annual riverine discharge of the present day Ob ( $917 \pm 264 \text{ pM}$ ,  $390 \text{ km}^3/\text{yr}$ ) and Yenisey ( $550 \pm 558 \text{ pM}$ ,  $620 \text{ km}^3/\text{yr}$ ) rivers, the two large rivers draining the Putoranan Plateau. For the unradiogenic end member, a lower concentration was assigned (65 pM) reflecting the modern Mackenzie River, the large river draining the

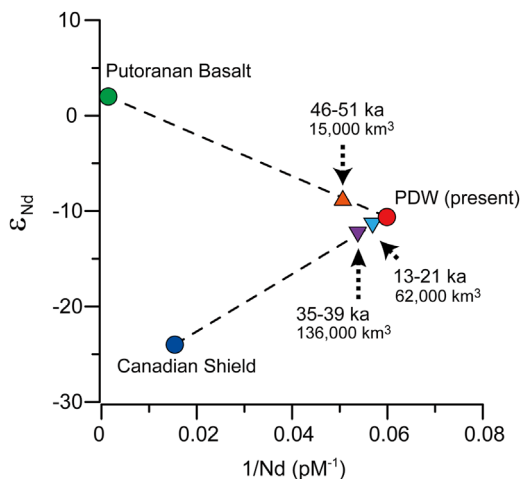


**Fig. 7.** Neodymium mixing diagram showing the three proposed end members: the Putoranan basalt sourced freshwater ( $[\text{Nd}] = 700 \text{ pM}$ ,  $\epsilon_{\text{Nd}} = +2$  from Sharma et al. (1992)) in green circle, the Canadian Shield sourced freshwater ( $[\text{Nd}] = 65 \text{ pM}$ ,  $\epsilon_{\text{Nd}} = -24$  from Winter et al. (1997)) in dark blue and the modern Polar Deep Water (PDW) ( $[\text{Nd}] = 16.7 \text{ pM}$ ,  $\epsilon_{\text{Nd}} = -10.63$  from Porcelli et al. (2009)) in red. The estimated volume of freshwater added to the PDW of the western Arctic Ocean are  $15,000 \text{ km}^3$  at 46–51 ka BP (orange triangle),  $136,000 \text{ km}^3$  at 35–39 ka BP (purple inverted triangle) and  $62,000 \text{ km}^3$  at 13–21 ka BP (light blue inverted triangle). (For interpretation of the references to color in this figure legend, the reader is referred to the web version of this article.)

Canadian Shield. The Nd concentrations were from the PARTNERS project (<http://arcticgreatrivers.org>) and the annual average discharges from Milliman and Farnsworth (2011). According to the mass balance calculation, the freshwater added to the PDW in the western Arctic were  $15,000 \text{ km}^3$  at 46–51 ka BP,  $136,000 \text{ km}^3$  at 35–39 ka BP and  $62,000 \text{ km}^3$  at 13–21 ka BP (Fig. 7). In our calculations, the freshwater input was considered to be an instantaneous event; had this persisted for longer time intervals, our estimates are minima.

For the 45–51 ka BP event, the source of freshwater was hypothesized to be in the eastern Arctic which made its way into the western Arctic surface water and eventually to the western Arctic PDW. If we assume for that event that 50% of the total volume released by ice dammed lakes flowed into the western Arctic Ocean as previously discussed in Section 3.3.1, this means that 60% of surface water was removed to PDW (Fig. 8). Although 60% of surface water sinking to form the PDW seems to be unrealistic in present day, it may have been possible during freshwater discharge events. Large freshwater input would have facilitated sea ice formation and brine rejection. Formation of sediment-loaded hyperpycnal flow by ice sheet collapse may also have contributed. In these cases, it is possible that shelf-water interaction and weathering of sediments in the hyperpycnal flow would have increased the Nd concentrations. Such increase in Nd concentrations was not considered, so our Nd concentrations for these freshwater endmembers are underestimates.

Extrapolating this fraction (60%) of PDW formation, the volumes of meltwater discharge at 35–39 ka BP and 13–21 ka BP would have been  $227,000 \text{ km}^3$  and  $103,000 \text{ km}^3$ , respectively (Fig. 8). The surface water transfer from the western to the eastern Arctic is assumed to be negligible because of the Beaufort Gyre and Transpolar Drift. Thus, at

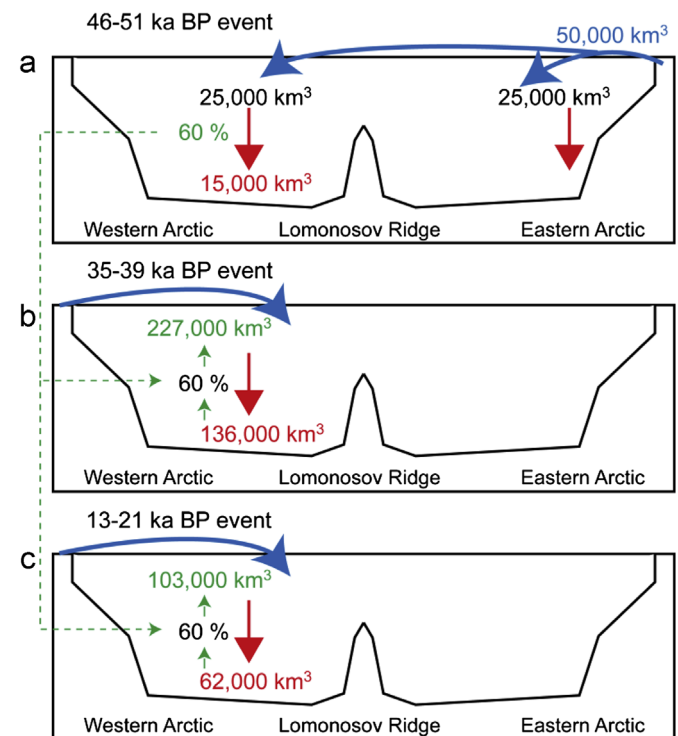


**Fig. 8.** Schematic illustration of (a) 46–51 ka BP, (b) 35–39 ka BP and (c) 13–21 ka BP freshwater discharge events with estimated freshwater volumes added to the western Arctic PDW (red). Dark blue arrows indicate the proposed pathway of three freshwater events in this study. (a) Using results of Nd mass balance calculation (red) and the estimated volume of ice dammed lakes (blue; Mangerud et al., 2004), the removal rate of surface water to the PDW was obtained (green). (b) and (c) The removal rate of 60% was applied to other periods of freshwater discharge and the volume of freshwater were estimated (green). (For interpretation of the references to color in this figure legend, the reader is referred to the web version of this article.)

most 91,000 and 41,000 km<sup>3</sup> of freshwater exited the Arctic ocean as surface water and directly fed the N. Atlantic at estimated 35–39 and 13–21 ka BP, respectively. The 91,000 km<sup>3</sup> of freshwater input from the Arctic to the North Atlantic, if unaccompanied by large amounts of iceberg transport, would have been only a minor component (~10%) of the estimated total freshwater flux during HE4 (~10<sup>6</sup> km<sup>3</sup> from Roche et al. (2004)).

From the 41,000 km<sup>3</sup> of freshwater input to the North Atlantic at estimated 13–21 ka BP, we speculate that it may be related to HE 1 (~30% of HE4 based on the volume of IRD, Hemming (2004)) rather than the outburst of Lake Agassiz during the Younger Dryas (Leverington et al., 2000). This is consistent with results from comparison of modeling and paleo-records (Bigg et al., 2011) that suggest that the Arctic, especially the LIS, contributed to HE1. Bigg et al. (2011) have inferred that Arctic sources also made significant contributions to the HE 2 (from LIS) and HE 3 (from northern Fennoscandian Ice Sheet). We do not expect HE3 to influence our site because of the surface circulation pattern in the Arctic, and we lack the resolution in our Nd isotope record to confirm or refute freshwater discharge events at either HE2 or HE3. The possibility also exists that the layer that we designated the CS may indeed represent a hiatus and that sediments deposited during HE 2 and HE 3 were eliminated as suggested by Poore et al. (1999) (Fig. 5).

#### 4. Conclusions

We reconstructed the variations in the Arctic circulation from measurements of authigenic neodymium isotopes in marine sediments on the Canada Basin side of the central Mendeleev Ridge. We found a radiogenic  $\epsilon_{\text{Nd}}$  peak at estimated 46–51 ka and unradiogenic peaks at estimated 35–39 and 13–21 ka BP. The peaks occurred at times of planktonic  $\delta^{18}\text{O}$  and  $\delta^{13}\text{C}$  depletions, and this correspondence indicates that  $\epsilon_{\text{Nd}}$  deviations resulted from freshwater additions. The three freshwater pulses recorded by authigenic neodymium isotopes concur in general with the end of middle Weichselian glaciation and Heinrich events 4 and 1. We infer that the radiogenic  $\epsilon_{\text{Nd}}$  peak accompanied by low inorganic carbon content at 46–51 ka BP reflects the outburst of ice-dammed lake systems in western Siberia affecting the PDW in the western Arctic Ocean through rearrangement in the surface circulation pattern. Meltwater discharge from LIS during HE4 was probably responsible for the unradiogenic  $\epsilon_{\text{Nd}}$  which coincided with an increase in inorganic carbon content at 35–39 ka BP. The unradiogenic  $\epsilon_{\text{Nd}}$  at 13–21 ka BP was possibly initiated by melting of LIS during HE1. These freshwater inputs containing weathering products of the two major glaciations influenced the PDW by brine formation and slope convection.

According to our very tentative mass balance calculations 50,000 km<sup>3</sup>, 227,000 km<sup>3</sup> and 103,000 km<sup>3</sup> of the freshwater input occurred in the Arctic Ocean at estimated 46–51, 35–39 and 13–21 ka BP, respectively. Of the total freshwater input 20,000 km<sup>3</sup>, 91,000 km<sup>3</sup> and 41,000 km<sup>3</sup> escaped deep water formation in the Arctic and directly fed the North Atlantic. The unradiogenic  $\epsilon_{\text{Nd}}$  peaks at estimated 35–39 and 13–21 ka BP correspond to intervals of proposed shutdown of NADW, but simple mass balance calculation implies that the contribution of the Arctic surface water to the abrupt global climate change during HE4 and HE1 could only have been minor. However, age uncertainty and sample resolution do not allow us to make a rigorous comparison.

#### Acknowledgments

This study was supported by the Polar Academic Program and K-Polar Project (PP12030) of KOPRI and the Mid-Career Researcher

Program (No. 2012-0005562) of NRF, MEST. We thank Dr. Y.-J. Jeong of KBSI for TIMS analyses. Comments from the editor and two anonymous reviewers improved the manuscript.

#### Appendix A. Supporting information

Supplementary data associated with this article can be found in the online version at <http://dx.doi.org/10.1016/j.epsl.2013.03.018>.

#### References

- Aagaard, K., Carmack, E.C., 1989. The role of sea ice and other fresh water in the Arctic circulation. *J. Geophys. Res.* 94, 14485–14498.
- Adler, R.E., Polyak, L., Ortiz, J.D., Kaufman, D.S., Channell, J.E.T., Xuan, C., Grotoli, A.G., Sellén, E., Crawford, K.A., 2009. Sediment record from the western Arctic Ocean with an improved Late Quaternary age resolution: HOTRAX core HLY0503-8JPC, Mendeleev Ridge. *Global Planet. Change* 68, 18–29.
- Aharon, P., 2006. Entrainment of meltwaters in hyperpycnal flows during deglaciation superstorms in the Gulf of Mexico. *Earth Planet. Sci. Lett.* 241, 260–270.
- Alkire, M.B., Falkner, K.K., Morison, J., Collier, R.W., Guay, C.K., Desiderio, R.A., Rigor, I.G., McPhee, M., 2010. Sensor-based profiles of the NO parameter in the central Arctic and southern Canada Basin: new insights regarding the cold halocline. *Deep-Sea Res.* 1 57, 1432–1443.
- Backman, J., Fornaciari, E., Rio, D., 2009. Biochronology and paleoceanography of late Pleistocene and Holocene calcareous nannofossil abundances across the Arctic Basin. *Mar. Micropaleontol.* 72, 86–98.
- Bayon, G., German, C.R., Boella, R.M., Milton, J.A., Taylor, R.N., Nesbitt, R.W., 2002. An improved method for extracting marine sediment fractions and its application to Sr and Nd isotopic analysis. *Chem. Geol.* 187, 179–199.
- Bigg, G.R., Levine, R.C., Green, C.L., 2011. Modelling abrupt glacial North Atlantic freshening: Rates of change and their implications for Heinrich events. *Global Planet. Change* 79, 176–192.
- Björck, G., Jakobsson, M., Rudels, B., Swift, J.H., Anderson, L., Darby, D.A., Backman, J., Coakley, B., Winsor, P., Polyak, L., Edwards, M., 2007. Bathymetry and deep-water exchange across the central Lomonosov Ridge at 88–89°N. *Deep-Sea Res.* 1 54, 1197–1208.
- Chester, R., Hughes, M.J., 1967. A chemical technique for the separation of ferromanganese minerals, carbonate minerals and adsorbed trace elements from pelagic sediments. *Chem. Geol.* 2, 249–262.
- Darby, D.A., Bischof, J.F., Spielhagen, R.F., Marshall, S.A., Herman, S.W., 2002. Arctic ice export events and their potential impact on global climate during the late Pleistocene. *Paleoceanography* 17 (2) 15–1–15–17 <http://dx.doi.org/10.1029/2001PA000639>.
- Darby, D.A., Ortiz, J.D., Grosch, C.E., Lund, S.P., 2012. 1500-year cycle in the Arctic Oscillation identified in Holocene Arctic sea-ice drift. *Nat. Geosci.* 5, 897–900.
- Darby, D.A., Polyak, L., Bauch, H.A., 2006. Past glacial and interglacial conditions in the Arctic Ocean and marginal seas—a review. *Prog. Oceanogr.* 71, 129–144.
- Dickson, R.R., Meincke, J., Malmberg, S.-A., Lee, A.J., 1988. The “Great Salinity Anomaly” in the northern North Atlantic 1968–1982. *Prog. Oceanogr.* 20, 103–151.
- Dokken, T.M., Jansen, E., 1999. Rapid changes in the mechanism of ocean convection during the last glacial period. *Nature* 401, 458–461.
- Fahl, K., Stein, R., 2012. Modern seasonal variability and deglacial/Holocene change of central Arctic Ocean sea-ice cover: new insights from biomarker proxy records. *Earth Planet. Sci. Lett.* 351–352, 123–133.
- Faure, G., Mensing, T.M., 2005. *Isotopes: Principles and Applications*. John Wiley & Sons Inc., Hoboken, New Jersey.
- Frank, M., Whiteley, N., Kasten, S., Hein, J.R., O’Nions, K., 2002. North Atlantic Deep Water export to the Southern Ocean over the past 14 Myr: evidence from Nd and Pb isotopes in ferromanganese crusts. *Paleoceanography* 17, 1022–1030.
- Grotes, P.M., Stuiver, M., 1999. GISP2 Oxygen Isotope Data. <http://dx.doi.org/10.1594/PANGAEA.56094>.
- Guay, C.K., Falkner, K.K., Muench, R.D., Mensch, M., Frank, M., Bayer, R., 2001. Wind-driven transport pathways for Eurasian Arctic river discharge. *J. Geophys. Res.* C: Oceans 106, 11469–11480.
- Gutjahr, M., Frank, M., Stirling, C.H., Klemm, V., van de Flierdt, T., Halliday, A.N., 2007. Reliable extraction of a deepwater trace metal isotope signal from Fe–Mn oxyhydroxide coatings of marine sediments. *Chem. Geol.* 242, 351–370.
- Haley, B.A., Frank, M., Spielhagen, R.F., Eisenhauer, A., 2007. Influence of brine formation on Arctic Ocean circulation over the past 15 million years. *Nat. Geosci.* 1, 68–72.
- Hanslik, D., Jakobsson, M., Backman, J., Björck, S., Sellén, E., O’Regan, M., Fornaciari, E., Skog, G., 2010. Quaternary Arctic Ocean sea ice variations and radiocarbon reservoir age corrections. *Q. Sci. Rev.* 29, 3430–3441.
- Hemming, S.R., 2004. Heinrich events: massive late Pleistocene detritus layers of the North Atlantic and their global climate imprint. *Rev. Geophys.* 42, RG1005, <http://dx.doi.org/10.1029/2003RG000128>.
- Hu, A., Meehl, G.A., Han, W., Timmermann, A., Otto-Bliesner, B., Liu, Z., Washington, W.M., Large, W., Abe-Ouchi, A., Kimoto, M., 2012. Role of the Bering Strait on the hysteresis

- of the ocean conveyor belt circulation and glacial climate stability. Proc. Natl. Acad. Sci. USA 109, 6417–6422.
- Hu, A., Meehl, G.A., Otto-Bliessner, B.L., Waelbroeck, C., Han, W., Loutre, M.F., Lambeck, K., Mitrovica, J.X., Rosenbloom, N., 2010. Influence of Bering Strait flow and North Atlantic circulation on glacial sea-level changes. Nat. Geosci. 3, 118–121.
- Jacobsen, S.B., Wasserburg, G.J., 1980. Sm–Nd isotopic evolution of chondrites. Earth Planet. Sci. Lett. 50, 139–155.
- Jakobsson, M., 2002. Hypsometry and volume of the Arctic Ocean and its constituent seas. Geochim. Geophys. Geosyst. 3, 1–18.
- Jakobsson, M., Løvlie, R., Al-Hanbali, H., Arnold, E., Backman, J., Mörth, M., 2000. Manganese and color cycles in Arctic Ocean sediments constrain Pleistocene chronology. Geology 28, 23–26.
- Jakobsson, M., Mayer, L., Coakley, B., Dowdeswell, J.A., Forbes, S., Fridman, B., Hodnesdal, H., Noormets, R., Pedersen, R., Rebesco, M., Schenke, H.W., Zaryayskaya, Y., Accettella, D., Armstrong, A., Anderson, R.M., Bienhoff, P., Camerlenghi, A., Church, I., Edwards, M., Gardner, J.V., Hall, J.K., Hell, B., Hestvik, O., Kristoffersen, Y., Marcussen, C., Mohammad, R., Mosher, D., Nghiem, S.V., Pedrosa, M.T., Travaglini, P.G., Weatherall, P., 2012. The International Bathymetric Chart of the Arctic Ocean (IBCAO) Version 3.0. Geophys. Res. Lett. 39, L12609, <http://dx.doi.org/10.1029/2012GL052219>.
- Jokat, W., 2009. The expedition of the research vessel “Polarstern” to the Arctic in 2008 (ARK-XXIII/3). Rep. Polar Mar. Res. 597, 1–222.
- Jones, E., Rudels, B., Anderson, L., 1995. Deep waters of the Arctic Ocean: origins and circulation. Deep-Sea Res. 42, 737–760.
- Keigwin, L.D., Donnelly, J.P., Cook, M.S., Driscoll, N.W., Brigham-Grette, J., 2006. Rapid sea-level rise and Holocene climate in the Chukchi Sea. Geology 34, 861–864.
- Knies, J., Matthiessen, J., Mackensen, A., Stein, R., Vogt, C., Frederichs, T., Nam, S.-I., 2007. Effects of Arctic freshwater forcing on thermohaline circulation during the Pleistocene. Geology 35, 1075–1078.
- Leverington, D.W., Mann, J.D., Teller, J.T., 2000. Changes in the bathymetry and volume of glacial lake Agassiz between 11,000 and 9300 <sup>14</sup>C yr B.P. Q. Res. 54, 174–181.
- Lisiecki, L.E., Raymo, M.E., 2005. A Plio-Pleistocene stack of 57 globally distributed benthic  $\delta^{18}\text{O}$  records. Paleoclimatology 20, PA1003, <http://dx.doi.org/10.1029/2004PA001071>.
- Miková, J., Denková, P., 2007. Modified chromatographic separation scheme for Sr and Nd isotope analysis in geological silicate samples. J. Geosci. 52, 221–226.
- Macdonald, R., Bewers, J., 1996. Contaminants in the arctic marine environment: priorities for protection. ICES J. Mar. Sci. 53, 537–563.
- Macdonald, R.W., Barrie, L.A., Bidleman, T.F., Diamond, M.L., Gregor, D.J., Semkin, R. G., Strachan, W.M.J., Li, Y.F., Wania, F., Alaea, M., Alexeeva, L.B., Backus, S.M., Bailey, R., Bewers, J.M., Gobeil, C., Halsall, C.J., Harner, T., Hoff, J.T., Jantunen, L.M. M., Lockhart, W.L., Mackay, D., Muir, D.C.G., Pudykiewicz, J., Reimer, K.J., Smith, J.N., Stern, G.A., Schroeder, W.H., Wagemann, R., Yunker, M.B., 2000. Contaminants in the Canadian Arctic: 5 years of progress in understanding sources, occurrence and pathways. Sci. Total Environ. 254, 93–234.
- Mangerud, J., Jakobsson, M., Alexanderson, H., Astakhov, V., Clarke, G.K.C., Henriksen, M., Hjort, C., Krinner, G., Lunke, J.-P., Möller, P., Murray, A., Nikolskaya, O., Saarnisto, M., Svendsen, J.I., 2004. Ice-dammed lakes and rerouting of the drainage of northern Eurasia during the Last Glaciation. Q. Sci. Rev. 23, 1313–1332.
- Matthiessen, J., Niessen, F., Stein, R., Naafs, B.D., 2010. Pleistocene glacial marine sedimentary environments at the eastern Mendeleev Ridge, Arctic Ocean. Polarforschung 79, 123–137.
- Matthiessen, J., Stein, R., 2008. Documentation of sediment core PS72/410-1. Alfred Wegener Institute, Bremerhaven—Polarstern core repository, <http://dx.doi.org/10.11594/PANGAEA.708027>.
- Milliman, J.D., Farnsworth, K.L., 2011. River Discharge to the Coastal Ocean: A Global Synthesis. Cambridge University Press, Cambridge.
- Morison, J., Kwok, R., Peralta-Ferriz, C., Alkire, M., Rigor, I., Andersen, R., Steele, M., 2012. Changing Arctic Ocean freshwater pathways. Nature 481, 66–70.
- Murton, J.B., Bateman, M.D., Dallimore, S.R., Teller, J.T., Yang, Z., 2010. Identification of Younger Dryas outburst flood path from Lake Agassiz to the Arctic Ocean. Nature 464, 740–743.
- Not, C., Hillaire-Marcel, C., 2012. Enhanced sea-ice export from the Arctic during the Younger Dryas. Nat. Commun. 3, 647, <http://dx.doi.org/10.1038/ncomms1658>.
- Peterson, B.J., Holmes, R.M., McClelland, J.W., Vörösmarty, C.J., Lammers, R.B., Shiklomanov, A.I., Shiklomanov, I.A., Rahmstorf, S., 2002. Increasing river discharge to the Arctic Ocean. Science 298, 2171–2173.
- Phillips, R.L., Grantz, A., 2001. Regional variations in provenance and abundance of ice-late clasts in Arctic Ocean sediments: implications for the configuration of ice-raftered Quaternary oceanic and atmospheric circulation in the Arctic. Mar. Geol. 172, 91–115.
- Pin, C., Zalduegui, J.S., 1997. Sequential separation of light rare-earth elements, thorium and uranium by miniaturized extraction chromatography: application to isotopic analyses of silicate rocks. Anal. Chim. Acta 339, 79–89.
- Piotrowski, A.M., Banakar, V.K., Scrivner, A.E., Elderfield, H., Galy, A., Dennis, A., 2009. Indian Ocean circulation and productivity during the last glacial cycle. Earth Planet. Sci. Lett. 285, 179–189.
- Polyak, L., Bischof, J., Ortiz, J.D., Darby, D.A., Channell, J.E.T., Xuan, C., Kaufman, D.S., Løvlie, R., Schneider, D.A., Eberl, D.D., Adler, R.E., Council, E.A., 2009. Late Quaternary stratigraphy and sedimentation patterns in the western Arctic Ocean. Global Planet. Change 68, 5–17.
- Polyak, L., Curry, W.B., Darby, D.A., Bischof, J., Cronin, T.M., 2004. Contrasting glacial/interglacial regimes in the western Arctic Ocean as exemplified by a sedimentary record from the Mendeleev Ridge. Palaeogeogr. Palaeoclimatol. Palaeoecol. 203, 73–93.
- Poore, R.Z., Osterman, L., Curry, W.B., Phillips, R.L., 1999. Late Pleistocene and Holocene meltwater events in the western Arctic Ocean. Geology 27, 759–762.
- Porcelli, D., Andersson, P.S., Baskaran, M., Frank, M., Björk, G., Semiletov, I., 2009. The distribution of neodymium isotopes in Arctic Ocean basins. Geochim. Cosmochim. Acta 73, 2645–2659.
- Reimer, P.J., Baillie, M.G.L., Bard, E., Bayliss, A., Beck, J.W., Blackwell, P.G., Ramsey, C. B., Buck, C.E., Burr, G.S., Edwards, R.L., 2009. IntCal09 and Marine09 radiocarbon age calibration curves, 0–50,000 years cal BP. Radiocarbon 51, 1111–1150.
- Rella, S.F., Uchida, M., 2011. Sedimentary organic matter and carbonate variations in the Chukchi Borderland in association with ice sheet and ocean–atmosphere dynamics over the last 155 kyr. Biogeosciences 8, 3545–3553.
- Risebrobakken, B., Balbon, E., Dokken, T., Jansen, E., Kissel, C., Labeyrie, L., Richter, T., Senneset, L., 2006. The penultimate deglaciation: high-resolution paleoceanographic evidence from a north–south transect along the eastern Nordic Seas. Earth Planet. Sci. Lett. 241, 505–516.
- Roche, D., Paillard, D., Cortijo, E., 2004. Constraints on the duration and freshwater release of Heinrich event 4 through isotope modelling. Nature 432, 379–382.
- Rudels, B., Anderson, L., Eriksson, P., Fahrback, E., Jakobsson, M., Jones, E.P., Melling, H., Prinsenber, S., Schauer, U., Yao, T., 2012. Observations in the Ocean. In: Lemke, H.-W., Jacobi, H.-W. (Eds.), Arctic Climate Change. Springer, Netherlands, pp. 117–198.
- Rutberg, R.L., Hemming, S.R., Goldstein, S.L., 2000. Reduced North Atlantic Deep Water flux to the glacial Southern Ocean inferred from neodymium isotope ratios. Nature 405, 935–938.
- Schlösser, P., Bönisch, G., Rhein, M., Bayer, R., 1991. Reduction of deepwater formation in the Greenland Sea during the 1980s: evidence from tracer data. Science 251, 1054–1056.
- Serreze, M.C., Barrett, A.P., Slater, A.G., Woodgate, R.A., Aagaard, K., Lammers, R.B., Steele, M., Moritz, R., Meredith, M., Lee, C.M., 2006. The large-scale freshwater cycle of the Arctic. J. Geophys. Res. 111, C11010, <http://dx.doi.org/10.1029/2005JC003424>.
- Sharma, M., Basu, A.R., Nesterenko, G., 1992. Temporal Sr-, Nd- and Pb- isotopic variations in the Siberian flood basalts: implications for the plume-source characteristics. Earth Planet. Sci. Lett. 113, 365–381.
- Spielhagen, R.F., Erlenkeuser, H., 1994. Stable oxygen and carbon isotopes in planktic foraminifers from Arctic Ocean surface sediments: reflection of the low salinity surface water layer. Mar. Geol. 119, 227–250.
- Spivack, A.J., Wasserburg, G.J., 1988. Neodymium isotopic composition of the Mediterranean outflow and the eastern North Atlantic. Geochim. Cosmochim. Acta 52, 2767–2773.
- Stein, R., Matthiessen, J., Niessen, F., Krylov, A., Nam, S., Bazhenova, E., 2010. Towards a better (litho-) stratigraphy and reconstruction of Quaternary paleoenvironment in the Amerasian Basin (Arctic Ocean). Polarforschung 79, 97–121.
- Stein, R., Nam, S.I.I., Schubert, C., Vogt, C., Futterer, D., Heinemeier, J., 1994a. The Last Deglaciation event in the Eastern Central Arctic Ocean. Science 264, 692–696.
- Stein, R., Schubert, C., Vogt, C., Futterer, D., 1994b. Stable isotope stratigraphy, sedimentation rates, and salinity changes in the Latest Pleistocene to Holocene eastern central Arctic Ocean. Mar. Geol. 119, 333–355.
- Stokes, C.R., Clark, C.D., 2003. Laurentide ice streaming on the Canadian Shield: a conflict with the soft-bedded ice stream paradigm? Geology 31, 347–350.
- Svendsen, J.I., Alexanderson, H., Astakhov, V.I., Demidov, I., Dowdeswell, J.A., Funder, S., Gataullin, V., Henriksen, M., Hjort, C., Houmark-Nielsen, M., Hubberten, H.W., Ingólfsson, Ó., Jakobsson, M., Kjær, K.H., Larsen, E., Lokrantz, H., Lunke, J.P., Lyså, A., Mangerud, J., Maitiouchkov, A., Murray, A., Möller, P., Niessen, F., Nikolskaya, O., Polyak, L., Saarnisto, M., Siegert, C., Siegert, M.J., Spielhagen, R.F., Stein, R., 2004. Late Quaternary ice sheet history of northern Eurasia. Q. Sci. Rev. 23, 1229–1271.
- Tachikawa, K., Jeandel, C., Roy-Barman, M., 1999. A new approach to the Nd residence time in the ocean: the role of atmospheric inputs. Earth Planet. Sci. Lett. 170, 433–446.
- Tarasov, L., Peltier, W., 2005. Arctic freshwater forcing of the Younger Dryas cold reversal. Nature 435, 662–665.
- Winter, B.L., Johnson, C.M., Clark, D.L., 1997. Strontium, neodymium, and lead isotope variations of authigenic and silicate sediment components from the Late Cenozoic Arctic Ocean: implications for sediment provenance and the source of trace metals in seawater. Geochim. Cosmochim. Acta 61, 4181–4200.
- Woodgate, R.A., Aagaard, K., Muench, R.D., Gunn, J., Björk, G., Rudels, B., Roach, A., Schauer, U., 2001. The Arctic Ocean boundary current along the Eurasian slope and the adjacent Lomonosov Ridge: water mass properties, transports and transformations from moored instruments. Deep-Sea Res. I 48, 1757–1792.